



# Oriented grain growth and modification of ‘frozen anisotropy’ in the lithospheric mantle

Yuval Boneh <sup>a,\*</sup>, David Wallis <sup>b</sup>, Lars N. Hansen <sup>b</sup>, Mike J. Krawczynski <sup>a</sup>, Philip Skemer <sup>a</sup>

<sup>a</sup> Washington University in St. Louis, Earth and Planetary Sciences, One-Brookings Drive, Campus Box 1169, Saint Louis, MO 63130, United States

<sup>b</sup> Oxford University, Department of Earth Sciences, Oxford, United Kingdom

## ARTICLE INFO

### Article history:

Received 14 April 2017

Received in revised form 25 June 2017

Accepted 29 June 2017

Available online xxxx

Editor: J. Brodholt

### Keywords:

olivine

crystallographic preferred orientation

grain growth

seismic anisotropy

mantle lithosphere

## ABSTRACT

Seismic anisotropy throughout the oceanic lithosphere is often assumed to be generated by fossilized texture formed during deformation at asthenospheric temperatures close to the ridge. Here we investigate the effect of high-temperature and high-pressure static annealing on the texture of previously deformed olivine aggregates to simulate residence of deformed peridotite in the lithosphere. Our experiments indicate that the orientation and magnitude of crystallographic preferred orientation (CPO) will evolve due to the preferential growth of grains with low dislocation densities. These observations suggest that texture and stored elastic strain energy promote a style of grain growth that modifies the CPO of a deformed aggregate. We demonstrate that these microstructural changes alter the orientation distributions and magnitudes of seismic wave velocities and anisotropy. Therefore, static annealing may complicate the inference of past deformation kinematics from seismic anisotropy in the lithosphere.

© 2017 The Authors. Published by Elsevier B.V. This is an open access article under the CC BY license (<http://creativecommons.org/licenses/by/4.0/>).

## 1. Introduction

The upper mantle is seismically anisotropic (e.g., Burgos et al., 2014), which is mainly attributed to elastically anisotropic olivine crystals aligned in a crystallographic preferred orientation (CPO) (e.g., Nicolas and Christensen, 1987). CPO in olivine is typically interpreted to result from solid-state plastic deformation. As such, interpretation of seismic anisotropy is the primary approach for inferring the kinematics of mantle flow (Karato et al., 2008; Skemer and Hansen, 2016).

The interpretation of seismic anisotropy is particularly challenging near plate boundaries, where flow patterns are complex (Boneh and Skemer, 2014; Skemer et al., 2012). However, even beneath the interiors of oceanic plates, which are assumed to be kinematically simple, there is still vigorous debate about the depths, magnitudes, and orientations of seismic anisotropy (Becker et al., 2014; Lin et al., 2016). Many studies assume that the orientation of anisotropy in the highly viscous lithospheric mantle is “locked-in” and records the kinematics of deformation during its formation at the mid-ocean ridge, while anisotropy in the asthenosphere is continuously overprinted by current plate motion. This basic model is supported by numerous studies that detect layered anisotropy in

both the oceanic and continental lithosphere (Barruol et al., 1997; Silver and Chan, 1991; Silver and Savage, 1994; Yuan and Romanowicz, 2010).

However, the validity of this model rests on two assumptions: first, that due to temperature-dependent changes in rock rheology the mantle does not deform significantly below a certain temperature, and second, that deformation is the only process that affects CPO. Here, we explore this second assumption by investigating the influence of high temperature and high pressure static annealing on the stability of olivine CPO.

## 2. Methods

The starting material for these experiments was a synthetic Fo<sub>50</sub> olivine aggregate, which was previously deformed in torsion at a confining pressure of 0.3 GPa and 1200 °C in a Pateron apparatus at the University of Minnesota (sample PT0718; for full description of the sample fabrication and deformation see: Hansen et al., 2016). Fo<sub>50</sub> is a reliable analogue to Fo<sub>90</sub> olivine in terms of its mechanical and textural behavior, but has a lower viscosity under the same deformation conditions, which facilitates high shear strain torsion experiments (Hansen et al., 2014; Zhao et al., 2009). We cut the deformed sample into three equal-sized slices along longitudinal sections parallel to both the radial direction and the axis of the initially cylindrical sample. As the sample was deformed in torsion, there is a linear gradient in shear strain from the outer edge to the center of the cylinder. The por-

\* Corresponding author.

E-mail addresses: boneh@levee.wustl.edu (Y. Boneh), david.wallis@earth.ox.ac.uk (D. Wallis), lars.hansen@earth.ox.ac.uk (L.N. Hansen), mikekraw@wustl.edu (M.J. Krawczynski), pskemer@wustl.edu (P. Skemer).

<http://dx.doi.org/10.1016/j.epsl.2017.06.050>

0012-821X/© 2017 The Authors. Published by Elsevier B.V. This is an open access article under the CC BY license (<http://creativecommons.org/licenses/by/4.0/>).

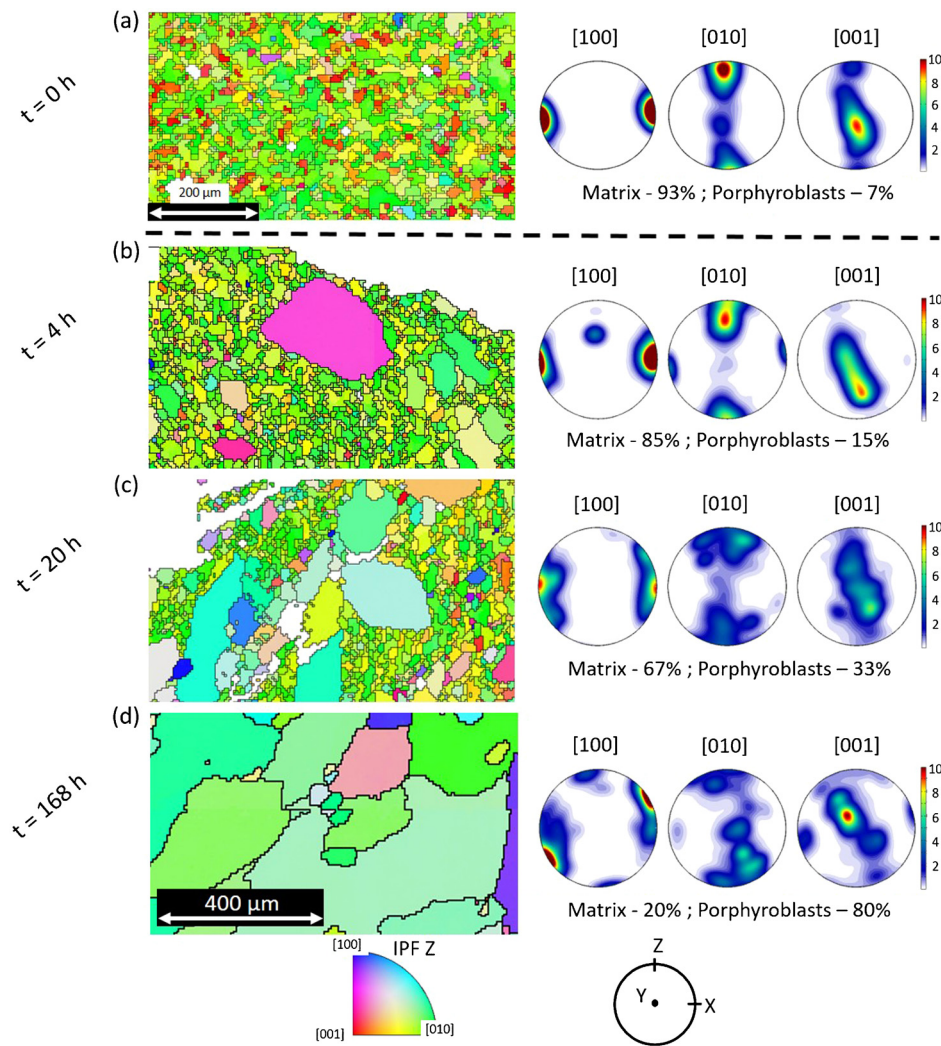


**Fig. 1.** Electron backscatter diffraction (EBSD) maps for (a) starting, initially deformed sample, and samples annealed for (b) 4 h, (c) 20 h, and (d) 168 h. Grain colors represent the orientation of the olivine crystal axes with respect to the normal to the shear plane (the Z-axis). Upper hemisphere pole figures show the associated crystallographic preferred orientation (CPO) of olivine where colors represent multiples of uniform distribution. Area fraction of matrix grains ( $d < 100 \mu\text{m}$ ) and porphyroblasts ( $d > 100 \mu\text{m}$ ) for each map is given in percentage beneath the corresponding pole figures.

tions of the sample used in this study were deformed to shear strains from  $\gamma = 7\text{--}10$ .

Following the torsional deformation, olivine grains in the sample are  $11 \pm 8 \mu\text{m}$  in diameter, with aspect ratios of approximately 2:1. The olivine CPO is strong, with [100] axes parallel to the shear direction and [010] axes perpendicular to the shear plane, which corresponds to the A-type CPO of Jung and Karato (2001) (Fig. 1a). The narrow size distribution of dynamically recrystallized grains, the strength of the CPO, and comparison to samples deformed to a wide range of strains in similar experiments suggest that the microstructure is near steady-state (Hansen et al., 2014).

In the annealing stage of the experiments, the samples were held at constant temperature and hydrostatic pressure, using  $\text{BaCO}_3$  and  $\text{MgO}$  as the pressure medium and spacers respectively, in a solid-medium piston-cylinder apparatus. Each sample was surrounded with  $\text{Fo}_{50}$  powder, which was identical to the powder used to synthesize the original sample, and packed inside a nickel capsule. The three samples were annealed at 1 GPa and  $1250^\circ\text{C}$  for 4, 20, or 168 h, respectively. During each run, pressure was increased to 1 GPa at room temperature and then temperature was increased by  $50^\circ\text{C}$  per min with a 6-min pause at  $900^\circ\text{C}$  to allow the system to stabilize. Samples were quenched by shutting off

the power to the furnace, which reduces the sample temperature to less than  $100^\circ\text{C}$  in under 30 seconds.

Thick sections of the annealed samples were prepared with a cross sectional area of  $\sim 1 \text{ mm}^2$  oriented parallel to the Y–Z plane of the starting deformed sample, i.e., within the plane that includes the radial direction (Y-axis) and the normal to the shear plane (Z-axis), and perpendicular to the shear direction (X-axis) (Fig. 1). Samples were polished using SiC and diamond abrasives down to 0.25 micron, followed by chemical–mechanical polishing using colloidal silica. Microstructural elements including grain size, intra- and inter-granular misorientation, and crystallographic orientation were characterized in two stages. First, large areas were mapped using conventional electron backscatter diffraction (EBSD). These data were acquired using a JEOL 7001-FLV scanning electron microscope (SEM) at 20 kV with an Oxford Instruments Nordlys F+ EBSD detector. Second, key areas were selected and mapped using high-angular resolution EBSD (HR-EBSD, Wallis et al., 2016; Wilkinson et al., 2006). These data were acquired using an FEI Quanta 650 field emission gun SEM at 30 kV with an Oxford Instruments Nordlys S EBSD detector. All data were acquired with SEMs operated in low-vacuum mode. EBSD maps have a step size of either 1 or 5 microns and HR-EBSD maps have a step size of  $0.6 \mu\text{m}$ . Data were analyzed using Oxford Instruments

Download English Version:

<https://daneshyari.com/en/article/5779746>

Download Persian Version:

<https://daneshyari.com/article/5779746>

[Daneshyari.com](https://daneshyari.com)